

Transparent glass-ceramics with (Eu³⁺,Yb³⁺):YNbO₄ nanocrystals: Crystallization, structure, optical spectroscopy and cooperative upconversion

P. A. Loiko¹, O. S. Dymshits^{2,*}, I. P. Alekseeva², A. A. Zhilin², M. Ya. Tsenter²,
E. V. Vilejshikova¹, K. V. Bogdanov³, X. Mateos⁴, and K. V. Yumashev¹

¹*Center for Optical Materials and Technologies (COMT), Belarusian National Technical University, 65/17 Nezavisimosti Ave., Minsk 220013, Belarus*

²*NITIOM Vavilov State Optical Institute, 36/1 Babushkin St, Saint-Petersburg 192171, Russia*

³*National Research University of Information Technologies, Mechanics and Optics, Kronverkskiy pr., 49, 197101 Saint-Petersburg, Russia*

⁴*Física i Cristal·lografia de Materials i Nanomaterials (FiCMA-FiCNA), Universitat Rovira i Virgili (URV), Campus Sescelades, C/ Marcel·li Domingo, s/n, Tarragona, Spain E-43007*

*Corresponding author e-mail: vodym@goi.ru, vodym1959@gmail.com

Abstract. In the present work, we report on a comprehensive study of crystallization, structure and optical spectroscopy of transparent glass-ceramics with (Eu³⁺,Yb³⁺):YNbO₄ nanocrystals synthesized by a secondary heat-treatment of Li₂O–Al₂O₃–SiO₂ glasses doped with rare-earth oxides and nucleated by Nb₂O₅, for the first time, to the best of our knowledge. Heat treatments result in volume crystallization of RENbO₄ with the sizes of 4 – 15 nm. Crystals of rare-earth niobates with disordered fluorite structure (T') appear during heat-treatment at 720–740 °C for 6 h, crystals with tetragonal structure (T) appear at higher temperatures or longer durations of heat-treatment, and at >1000 °C the transformation to a monoclinic form (M) begins. Rare-earth niobates act as nucleating agents for bulk crystallization of β-quartz solid solutions, the main crystalline phase of the glass-ceramics. Optical spectroscopy confirms entering of both Eu³⁺ and Yb³⁺ ions into the RENbO₄ nanophase and their spectroscopic properties changes according to the T' → T → M phase transformations. Under UV excitation, glass-ceramics heat-treated at 900 °C provide intense red emission with the color coordinates $x = 0.665$, $y = 0.335$ (CIE 1931). At 1000 °C, a partial reduction of Eu³⁺ to Eu²⁺ is observed which allows for tuning of color properties of emission. When excited in the near-IR by an InGaAs diode, the initial glass and glass-ceramics show red cooperative upconversion due to the 2Yb³⁺ → Eu³⁺ energy transfer. The efficiency of the latter is ~10%. The developed materials due to the good emission and thermo-mechanical properties are promising for the development of color-tunable red phosphors.

Keywords: glass-ceramics; orthoniobates; europium; ytterbium; luminescence; up-conversion

1. Introduction

The electronic configuration of Eu is $[\text{Xe}]4f^75d^06s^2$, where $[\text{Xe}]$ represents the electronic configuration of Xenon. Europium is a polyvalent ion. Trivalent europium ions, Eu^{3+} , attract a lot of attention due to their intense emission related to $^5\text{D}_0 \rightarrow ^7\text{F}_J$ transitions within the $4f^6$ electronic shell. Efficient red and orange-red phosphors with Eu^{3+} ions such as the commercial yttrium oxide, $\text{Eu}:\text{Y}_2\text{O}_3$ [1,2], are used in tricolour lamps, field emission displays, cathode-ray tubes and solid-state lighting; while Eu^{3+} -doped single-crystals, e.g. $\text{KGd}(\text{WO}_4)_2$, are promising for deep-red (~ 703 nm) lasers [3].

Luminescent properties of Eu^{3+} ions are sensitive to their site symmetry [4-6]. Thus, Eu^{3+} ions are frequently used as structural probes by monitoring a hypersensitive electric-dipole, ED, transition $^5\text{D}_0 \rightarrow ^7\text{F}_2$. In addition, a reduction from Eu^{3+} to Eu^{2+} [7-10] can be observed under some conditions, i.e., heat-treatment or reducing atmosphere of synthesis. Different from Eu^{3+} , the Eu^{2+} ions feature the parity allowed interconfigurational $[\text{Xe}]4f^7 \leftrightarrow [\text{Xe}]4f^65d^1$ transitions, divalent europium ion produces blue emission centered at ~ 450 nm with a characteristic afterglow. It is used in commercial blue phosphors, such as $\text{BaMgAl}_{10}\text{O}_{17}$ [11]. Various dielectric hosts in the form of nano-powders [12-16], films [17-19], crystals [20-22], glasses [23-27] and glass-ceramics (GCs) [28-37] were studied for Eu-doping to improve the emission efficiency, as well as to tune the color properties; and the list is ever growing.

In addition to direct UV-excitation, red europium luminescence can be excited with InGaAs diodes emitting at ~ 980 nm via the so-called cooperative energy transfer from an excited pair of Yb^{3+} ions to a single Eu^{3+} ion in $(\text{Eu}^{3+}, \text{Yb}^{3+})$ codoped materials. Phosphors based on Y_2O_3 [38,39], $\text{Y}_3\text{Al}_5\text{O}_{12}$ and $\text{Gd}_3\text{Ga}_5\text{O}_{12}$ [40], $\text{Li}_2\text{Lu}_5\text{O}_4(\text{BO}_3)_3$ [41] and BaB_4O_7 [42] nano-powders codoped with Eu^{3+} and Yb^{3+} were previously studied, as well as $\text{Eu}:\text{KYb}(\text{WO}_4)_2$ single crystal [43]. Also, $(\text{Eu}^{3+}, \text{Yb}^{3+})$ codoped oxyfluoroborate [44], oxyfluoride [45,46], sol-gel silica [47] and fluorotellurite [48] glasses are known. Transparent nanophase GCs could be a good alternative to glasses, single crystals and nano-powders due to a simple method of their synthesis based on conventional glass technology, i.e. melt-quenching with subsequent heat-treatments. GCs also can provide enhancement of luminescent properties of RE ions when these ions enter the nanocrystals. However, there are only few reports about the $\text{Yb}^{3+} \rightarrow \text{Eu}^{3+}$ energy transfer in GCs: oxyfluoride GCs based on the $\text{Eu}^{3+}, \text{Yb}^{3+}:\text{PbF}_2$ or SrF_2 nano-phases were studied in [49], Eu/Yb codoped ZnO nanocrystals embedded in B_2O_3 glass matrix were reported in [50]. $(\text{Eu}^{3+}, \text{Yb}^{3+})$ codoped GCs developed for down-conversion based on reverse energy transfer process, $\text{Eu}^{3+} \rightarrow \text{Yb}^{3+}$, are also known [51,52].

Yttrium orthoniobate, YNbO_4 , is a self-activated X-ray phosphor widely used in X-ray medical imaging, in computed radiography, tomography and fluoroscopy [53]. YNbO_4 is an excellent luminescent host because yttrium ions are easily replaced by other rare-earth ions. For instance, Eu^{3+} -doped yttrium orthoniobate, Eu:YNbO_4 , is a promising luminescent material [12,54-60]. 5 at% $\text{Yb}^{3+}:\text{YNbO}_4$ crystal was grown; results of its study suggested that it is a potential all-solid-state pumped laser crystal in tunable and ultrafast lasers field [61]. Previous studies [62,63] were focused also on pure EuNbO_4 synthesized in the form of nano-, poly- and single crystals and on YbNbO_4 [64]. Appearance of YbNbO_4 was demonstrated in NaNbO_3 nanocrystals prepared by a sol-gel method; the spectral-luminescent properties of YbNbO_4 crystals were studied in [64].

For rare-earth orthoniobates, RENbO_4 , there are two common crystalline forms, the low temperature M-phase isostructural with the monoclinic form of the mineral fergusonite, $(\text{R}^{3+})(\text{Nb,Ta})\text{O}_4$ [65] and the high temperature T-phase corresponding to a distorted version of the tetragonal scheelite (CaWO_4) structure [66]. The transition between the two phases occurs reversibly in the range 500-800 °C, depending on the rare earth ion. In both polymorphs, the rare-earth ions are inside a deformed polyhedron with the coordination 8 whereas the Nb^{5+} ions occur inside an irregular distorted tetrahedron of oxygens [65,67]. Heating of the specimen close to the melting temperature results in a high temperature cubic phase [66]. This phase has a random cation distribution in a fluorite-type structure (T'-phase) [68].

Glass-ceramics with rare-earth ions embedded into crystalline phases are intensively studied due to the search for new efficient photoluminescent and up-conversion multifunctional materials. Combination of unique thermal-mechanical properties of lithium aluminosilicate (LAS) glass-ceramics and their transparency with optical properties of rare-earth ions allows developing multifunctional materials. Recently, we developed transparent GCs with $(\text{Er,Yb})\text{NbO}_4$ and YbNbO_4 orthoniobate nanocrystals by secondary heat-treatments of the initial LAS glass doped with Nb_2O_5 and Er and/or Yb oxides [69]. Here, for the first time we report the preparation of transparent glass-ceramics containing Eu^{3+} , Yb^{3+} -codoped yttrium orthoniobate nanocrystals by the melt-quenching method. Their structure, optical absorption and visible luminescence under direct excitation of the Eu^{3+} ions by a blue GaN diode, as well as under near-IR excitation by an InGaAs diode via the $2\text{Yb}^{3+} \rightarrow \text{Eu}^{3+}$ cooperative energy-transfer process were studied.

2. Experimental

The glass with the composition of 18 Li₂O, 27 Al₂O₃ and 55 SiO₂ (mol%) [69,70] was chosen for the study. It was doped with 0.5 mol% Eu₂O₃, 1.7 mol% Yb₂O₃, 1.0 mol% Y₂O₃ and 3.2 mol% Nb₂O₅.

Batch to produce 300 g of glass was melted in a crucible made of quartz ceramics in a laboratory electric furnace at 1580 °C for 4 h with stirring, then the glass melt was bubbled by oxygen for 0.5 h to remove the hydroxyl groups from the melt. The melt was poured onto a metal plate and the initial glass was annealed at 620 °C. Then it was heat-treated in isothermal conditions in the temperature range from 680 to 1100 °C for 6 - 24 h.

Differential scanning calorimetry (DSC) measurements were performed by means of a the simultaneous thermal analyzer NETZSCH STA 449 F3 Jupiter[®] in platinum crucibles, in the temperature range from room temperature to 1100 °C at a heating rate of 10 K/min in Ar, on the bulk sample of 17 mg.

X-ray diffraction (XRD) patterns of powdered initial glass and glass-ceramic samples were measured using a Shimadzu XRD-6000 diffractometer, Cu K_α radiation with a Ni filter. The mean crystal sizes were estimated from broadening of X-ray peaks according to Scherrer's equation:

$$D = K\lambda/\Delta(2\theta)\cos\theta, \quad (1)$$

where λ is the wavelength of X-ray radiation, θ is the diffraction angle, $\Delta(2\theta)$ is the width of peak at half of its maximum, and K is a dimensionless number known as the Scherrer constant. In general, K depends both on the shape of the crystal particles and on the order of XRD spectrum. If the particles are spherical, which is our case according to the TEM studies of the glass-ceramic samples (see below), K , by symmetry, will be the same for all orders ($K = 1.0747$) [71]. For the consistency with our previous studies, we will take $K \equiv 1$ and specify the error in the mean crystal size estimation as ~10%.

The structure of the initial glass and glass-ceramics was studied with the transmission electron microscopy (TEM). The microscope used was JEOL TEM-1011 (100 kV acceleration voltage, 0.4 nm point resolution). For TEM studies, finely powdered samples dispersed in ethanol were used.

For the spectroscopic studies, thin (2 mm) polished plates of initial glass and glass-ceramics were used.

Raman spectra were recorded in backscattering geometry by an InVia (Renishaw, England) Micro-Raman spectrometer equipped with the multichannel detector cooled up to -70 °C. According to findings of K.P.F. Siqueira et al. [72], the best Raman spectra are obtained for Eu and Er niobates using the blue excitation line (488 nm) while green excitation line (514.5 nm) is suitable for Ho and Yb

niobates. This allows to avoid luminescence connected with strong electronic transitions of corresponding rare-earth ions [72]. Keeping it in mind, all samples were submitted to two different Raman excitation lines as they contain both Eu and Yb ions. So, Ar⁺ laser lines of 488 and 514 nm were employed as excitation sources. Leica 50^x (N.A. = 0.75) objective was used for illuminating the sample; the scattered light was collected by the same objective. Notch filter was placed before the spectrograph entrance slit; a spatial resolution was of 2 cm⁻¹ and acquisition time was 60 s.

Optical absorption spectra were measured in the spectral range of 0.35–3.00 μm with a Varian CARY-5000 spectrophotometer, the spectral bandwidth (SBW) was 0.1 nm.

Visible luminescence of Eu³⁺ ions was excited at 400 nm by a blue GaN diode. The near-IR Yb³⁺ luminescence, as well as upconversion luminescence (UCL) from the Yb³⁺–Eu³⁺ couple was excited by a focused radiation of 960 nm InGaAs laser diode. All emissions were collected by a wide-aperture lens and reimaged to the input slit of the monochromator MDR-23 (SBW = 0.5 nm). The spectrum was detected with a lock-in amplifier and InGaAs Hamamatsu G5851 (in the near-IR) or Hamamatsu C5460-01 (in the visible) photodetector. For UCL studies, the output power of the laser diode was scaled to determine the UCL intensity vs. excitation power plots.

The decay of 1 μm Yb³⁺ emission (excited at 960 nm by means of ns output from the optical parametric oscillator, OPO), was detected with a monochromator MDR-12, the G5851 photodetector and 500 MHz Tectronix TDS-3052B digital oscilloscope. For the measurement of Yb³⁺ lifetime, fine powdered samples immersed in glycerin were used (in order to exclude the impact of self-trapping). For the decay measurements in the visible range (Eu³⁺ emission), OPO was tuned to 532 nm, and fast Hamamatsu C5460 photodiode was used.

3. Results

The initial glass and samples obtained by heat-treatments at 700 – 740 °C for 6 h were transparent; they became slightly haze after heat-treatment at 740 °C for 24 h, the opalescence increased with increasing the heat-treatment temperature (Fig. 1).

3.1. DSC, XRD and TEM study

Fig. 2 shows the DSC curve obtained during heating for the initial glass. The thermogram exhibited a weak glass transition T_g with inflection point at 706 °C. Three exothermic peaks indicate the presence of different crystalline phases in the samples. The first broad exothermic peak appears at T_{x1}

= 818 °C, where T_{x1} is a crystallization-beginning temperature. It is followed by the sharp intense peak at $T_{x2} = 858$ °C and accompanied by a small broad peak with $T_{x2} = 920$ °C.

The XRD patterns for the initial and heat-treated glasses are presented in Fig. 3. Initial glass, as well as the glasses heat-treated at 700 °C and 720 °C are X-ray amorphous (Fig. 3a). Crystals of Eu,Yb:YNbO₄ orthoniobate with disordered fluorite-type structure (T'-phase) 4 nm in size evolve in the course of heat-treatment at 740 °C for 6 h, the prolongation of heat-treatment at this temperature results in increasing fraction of the orthoniobate phase (its structure becomes the tetragonal one) and in volume crystallization of β -quartz solid solution (Fig. 3b); the glass-ceramic samples become slightly haze (Fig. 1). Thus, nanocrystals of rare-earth orthoniobates serve as the heterogeneous nucleation sites for the crystallization of β -quartz solid solution (ss). The crystallinity fraction and crystal sizes increase with heat-treatment. After heat-treatment at 900 °C for 6 h, the size of tetragonal crystals of Eu,Yb:YNbO₄ (T-phase) is 12 nm, the size of β -quartz ss is about 50 nm. XRD pattern of the sample heat-treated at 1000°C for 6 h evidences co-precipitation of tetragonal and monoclinic nanocrystals (M-phase) of Eu,Yb:YNbO₄ together with β -quartz ss (Fig. 3a). The sample is translucent (Fig. 1).

Fig. 4 shows the TEM images of the glass-ceramic samples prepared by heat-treatments at 800 and 900 °C for 6 h. Both images demonstrate near the uniform distribution of dark regions of inhomogeneity without any clustering; their sizes and fraction increase with the heat-treatment temperature. The sizes of these dark regions of inhomogeneity are about 9 ± 2 nm in glass-ceramics obtained by the heat-treatment at 800 °C for 6 h, the average sizes are about 12 ± 2 nm in glass-ceramics prepared at 900 °C for 6 h. The observed change of the color intensity of dark regions of inhomogeneity presumably is due to their different distance from the sample surface. The similarity of sizes of these regions and the sizes of Eu,Yb:YNbO₄ crystals imply that these regions are crystals of rare-earth niobates.

3.2 Raman spectra

Raman spectra of the initial and heat-treated glasses are shown in Figs. 5a ($\lambda_{ex} = 488$ nm) and 5b ($\lambda_{ex} = 514$ nm). The comparison of Raman spectra collected at two different wavelengths allows us to find the bands connected with luminescence of rare-earth ions. For $\lambda_{ex} = 488$ nm, they are located in the range of $900 - 1100$ cm⁻¹, the peaks become distinct after heat-treatment at 1000 °C and correspond to the following wavelengths: 886 cm⁻¹– 510.1 nm, 923 cm⁻¹–510.9 nm, 948 cm⁻¹– 511.7 nm, 974 cm⁻¹– 512.3 nm and 1000 cm⁻¹– 513.1 nm.

For $\lambda_{\text{ex}} = 514 \text{ nm}$, the luminescence bands are located in the range of $1300 - 1400 \text{ cm}^{-1}$ for all the samples, at $550 - 770 \text{ cm}^{-1}$ (spectra for initial glass and samples heat-treated at 720 and $740 \text{ }^\circ\text{C}$ for 6 h) and at 860 cm^{-1} (the spectrum for glass heat-treated at $1000 \text{ }^\circ\text{C}$ for 6 h). They correspond to the following wavelengths: $616 \text{ cm}^{-1} - 531.4 \text{ nm}$, $760 \text{ cm}^{-1} - 535.5 \text{ nm}$, $860 \text{ cm}^{-1} - 538.4 \text{ nm}$, $1341 \text{ cm}^{-1} - 552.7 \text{ nm}$, $1345 \text{ cm}^{-1} - 552.8 \text{ nm}$. Additional bands are related to the visible emissions from impurity Er^{3+} ions presented in Yb_2O_3 reagent (see also section 3.5). It should be noted that the intensity and splitting of these emissions increase significantly for heat-treatment temperature of $800\text{-}1000 \text{ }^\circ\text{C}$, which indicates that Er^{3+} ions enter the niobate crystals [69].

The spectrum of the initial glass demonstrates two broad intense bands at $\sim 487\text{-}500 \text{ cm}^{-1}$ and at $870\text{-}895 \text{ cm}^{-1}$, of which the band 870 cm^{-1} is more intense (Fig. 5). The weak broad band at $\sim 295 \text{ cm}^{-1}$ is superimposed on the first band while the second one has a shoulder at about $\sim 970 \text{ cm}^{-1}$ (Fig. 5(b)). After heat treatment at $720 \text{ }^\circ\text{C}$ for 6 h the spectrum resembles that of the initial glass. Indeed, the low-frequency part of the spectrum remains unchanged, however, the shape of the left side of the high-frequency band slightly changes due to increasing intensity at about 817 cm^{-1} (or about 805 cm^{-1}). The difference in frequencies of these bands reflects the superposition of luminescence bands (Fig. 5(b)). Intensity of the high-frequency band at 817 cm^{-1} for $\lambda_{\text{ex}} = 488 \text{ nm}$ (at 805 cm^{-1} for $\lambda_{\text{ex}} = 514 \text{ nm}$) in the Raman spectrum of the sample heat-treated at $740 \text{ }^\circ\text{C}$ for 6 h (Fig. 5) increases. Intensity of the weak broad band at $\sim 295 \text{ cm}^{-1}$ also slightly increases.

The Raman spectrum drastically changes after heat-treatment at $800 \text{ }^\circ\text{C}$ for 6 h . This heat-treatment results in the diminishing of the broad band at 870 cm^{-1} and of a shoulder at about $\sim 970 \text{ cm}^{-1}$ and in the appearance of the intensive band at 807 cm^{-1} and a band at about 1085 cm^{-1} . A narrow and intense band at 482 cm^{-1} arises instead of the broad band $\sim 490 \text{ cm}^{-1}$, and weak bands are distinguished at $114\text{-}120$, 200 , 250 , 340 and 658 cm^{-1} (Fig. 5). With increasing the heat-treatment temperature to $1000 \text{ }^\circ\text{C}$, there is a strengthening and narrowing of almost all bands and a shift of the bands 250 to 238 cm^{-1} and 340 to 330 cm^{-1} . Simultaneously new Raman bands appear at $\sim 420 \text{ cm}^{-1}$ (the shoulder of the band at 482 cm^{-1}) and at 695 cm^{-1} (Fig. 5).

3.3 Optical absorption

The room temperature absorption spectra of the initial glass and glass-ceramics were recorded and shown in Fig. 6. The absorption spectrum is due to Eu^{3+} ions except a broad and intense band at $850\text{-}1050 \text{ nm}$, which is due to Yb^{3+} ions (${}^2\text{F}_{5/2} \rightarrow {}^2\text{F}_{7/2}$). The absorption bands are assigned to electronic

transitions from the 7F_0 ground state and thermally populated lower-lying 7F_1 excited state to different higher-lying excited states of Eu^{3+} : ${}^7F_{0,1} \rightarrow {}^5L_6$ (~ 395 nm), ${}^7F_0 \rightarrow {}^5D_2$ (~ 465 nm), ${}^7F_{0,1} \rightarrow {}^5D_1$ (~ 530 nm), ${}^7F_{0,1} \rightarrow {}^7F_5 + {}^7F_6$ (1800–2250 nm) on the basis of earlier work [73]. In the mid-IR, a sharp peak at ~ 3 μm is related to the absorption of OH⁻-groups. In Fig. 6, the Fresnel losses were subtracted. For this, the refractive indices n of the initial glass and glass-ceramics were first measured at ... ($n = \dots$ for the initial glass and $n = \dots$ for the sample heat-treated at 900 °C) and then the values of n at different wavelengths were estimated from the dispersion of the Fresnel losses in the transparency ranges. Finally, the losses in the glass and glass-ceramic samples are < 0.05 cm^{-1} in the near-IR (at ~ 1.5 μm).

For the initial glass and glass-ceramics, the most intense absorption band of Eu^{3+} ions at about 395 nm related to the transition ${}^7F_0 \rightarrow {}^5L_6$ is shown in Fig. 7(a). It is suitable for the excitation of the red Eu^{3+} emission by GaN laser diodes emitting around ~ 400 nm. For the initial glass, the band is centered at 393.8 nm; the corresponding peak absorption coefficient $\alpha = 0.5$ cm^{-1} (the background losses are extracted). The heat-treatment of the initial glass at 740 °C for 24 h or at 800–900 °C for 6 h results in a substantial enhancement of the peak absorption ($\alpha = 2.3$ cm^{-1}), red-shift of the peak to 395.3 nm, as well as its narrowing, with the full width at half maximum (FWHM) being < 0.9 nm. A weak shoulder centered at ~ 397 nm and related to the less intense transition ${}^7F_1 \rightarrow {}^5L_6$ is also resolved. All these changes indicate that Eu^{3+} ions for samples heat-treated at 740 °C for 24 h and at 800 - 900 °C for 6 h enter the T-YNbO₄ nanocrystals. For the samples heat-treated at 720–740 °C for 6 h, the above mentioned band contains two components emerging from the absorption of Eu^{3+} ions remaining in the residual glassy phase, as well as ones entering the T'-phase nanocrystals with fluorite structure.

In the higher wavelength spectral range, the relatively intense absorption bands of Eu^{3+} ions are also detected, see Fig. 7(b,c). They are related to the ${}^7F_0 \rightarrow {}^5D_2$ and the ${}^7F_{0,1} \rightarrow {}^5D_1$ transitions. For the initial glass, the first band is centered at 464.3 nm; the heat-treatment at 900 °C induces the increase of peak absorption (to ~ 0.7 cm^{-1}) and its splitting, 465.8 and 466.1 nm (related to the increased Stark splitting for the nano-crystalline Eu-doped T-phase of RE orthoniobate). The second band is also structured, with the components at 527.6 (transition from the 7F_0 state) and 536.3 and 538.5 nm (transition from the 7F_1 state); however, the peak absorption remains near unchanged. The spectrum of the sample heat-treated at 720 °C indicates just the beginning of the crystallization of Eu-doped disordered T'- orthoniobate phase; and the heat-treatment at 740 °C for 6 h corresponds to a near-equal distribution of Eu^{3+} ions over a glassy and a crystalline phases. Absorption at 1.75–2.3 μm refers to the transitions to the lower-lying excited states of Eu^{3+} ions, 7F_6 and 7F_5 . At 2100 and 2200 nm one can see

the europium transitions, ${}^7F_0 \rightarrow {}^7F_6$ and ${}^7F_1 \rightarrow {}^7F_6$, respectively. Structuring of these absorption bands and redistribution of their intensities is observed after heat-treatments at 740 °C for 24 h and at 800 and 900 °C for 6 h (Fig. 9).

Figure 8 shows the characteristic band of Yb^{3+} ions related to the ${}^2F_{7/2} \rightarrow {}^2F_{5/2}$ transition, for the initial glass and glass-ceramics. For the glass, the spectrum contains intense peak at 976.0 nm ($\alpha = 7.9 \text{ cm}^{-1}$), as well as a wide and non-structured plateau at shorter wavelengths. There is a negligible spectral change after heat-treatments at 700 and at 720 °C for 6 h. The spectrum changes more pronouncedly after heat-treatment at 740 °C for 6 h: Intensity of the peak at 976.0 nm exhibits a slight blue-shift and diminishes while the plateau narrows and gets a structure; its intensity slightly increases. Heat-treatment at 740 °C for 24 h, as well as at 800 °C for 6 h and at 900 °C for 6 h induces a blue-shift of the most intense peak to 974.8 nm and the decrease of the related absorption coefficient to 5.2 cm^{-1} . The structuring and rise of the plateau with the local peaks 915, 929 and 950 nm is seen; together with better resolved local peaks at 1004 and 1023 nm. The similar peaks positions were observed for 5 at% $\text{Yb}^{3+}:\text{YNbO}_4$ crystal grown by Czochralski method [61]: absorption peaks were located at 933, 955, 974 and 1003 nm. This indicates that Yb^{3+} ions (similar to Eu^{3+} ones) enter the RENbO_4 nanocrystals. Similarly, for the heat-treatment at 720–740 °C for 6 h, Yb^{3+} ions partly remain in the residual glassy phase, partly enter the T' - RENbO_4 nanocrystals.

Referring to the approach presented by P. Naresh [74], we calculated the optical band gap energy for the initial glass and glass-ceramics from the UV absorption edge using the well-known Tauc law relation [75]. From the observed absorption edges, we have evaluated the optical band gap energies (E_{op}) of these samples by plotting $(\alpha h\nu)^2$ vs. energy ($h\nu$) as shown in the inset in Fig. 6 where α is the absorption coefficient, $h\nu$ is the incident photon energy, 2 is constant, corresponding to direct allowed transitions. The values of E_{op} are determined from the linear region of the curve after extrapolating to meet the axis $h\nu$. Heat-treatments induce continuous red-shift of position of the UV absorption edge from 338 nm ($E_{\text{op}} = 3.67 \text{ eV}$) for the initial glass to 353 nm ($E_{\text{op}} = 3.51 \text{ eV}$). The value of $E_{\text{op}} = 3.51 \text{ eV}$ corresponds well with the value of $E_{\text{op}} = 3.4\text{--}3.6 \text{ eV}$ obtained for the solid solutions with the monoclinic structure in the $\text{YNbO}_4\text{--EuNbO}_4$ system [60].

3.4 Luminescence

Photoluminescence (PL) spectra of Eu^{3+} ions in the initial glass and glass-ceramics upon direct excitation the ${}^7F_0 \rightarrow {}^5L_6$ transition at $\sim 400 \text{ nm}$ are shown in Fig. 9a. The PL intensity for all samples

was normalized to unity in order to monitor the changes in the PL spectra with the heat-treatment. Observed PL bands are related to transitions from the 5D_0 metastable excited state to the 7F_J ones.

For the initial glass, the bands are centered at 579 (0→0), 591 (0→1), 613 (0→2), 652 (0→3) and 702 nm (0→4). The *Commission internationale de l'éclairage*, CIE 1931, coordinates for the glass phosphor are $x = 0.659$, $y = 0.341$ that falls into the red region. The dominant wavelength is 608 nm with the 0.99 purity. PL spectra of samples prepared by heat-treatments at 700 – 740 °C for 6 h are similar to that of the initial glass (Fig. 9a). The narrowing and splitting of PL bands of samples heat-treated at 740 °C for 24 h, at 800 or 900 °C for 6 h is in agreement with the increased Stark splitting for Eu^{3+} ions entering the nanocrystals. An increase of the volume fraction of T-(Y,Yb,Eu)NbO₄ phase with increase of the heat-treatment temperature in the range 720–900 °C is clearly seen in PL spectra of the glass-ceramics. For the sample heat-treated at 900 °C, the forbidden 0→0 transition is not detected; the 0→1 band is centered at 593.6 nm, the 0→2 band is split in two components, 612.6 and 614.1 nm, the 0→3 band is very weak and appears at ~655 nm; and the 0→4 band is also split, 694.7 and 704.4 nm. For the sample heat-treated at 900°C, CIE coordinates are $x = 0.665$, $y = 0.335$ (red emission); the dominant wavelength is 610 nm and the color purity is 0.99.

The heat-treatment at 1000 °C (the beginning of precipitation of monoclinic RE niobate phase) leads to further modification of the PL spectrum, see Fig. 9b. The band 0→1 contains two local peaks at 591.8 and 594.5 nm; the 0→2 band is split in 3 local peaks, 612.0, 613.6 and 614.5 nm; the 0→3 band is extremely weak; the 0→4 band is split in two peaks, at 705.0 and 705.8 nm. More important that this heat-treatment induces the $Eu^{3+} \rightarrow Eu^{2+}$ reduction; and blue emission of divalent europium is observed, see inset in Fig. 9b. The band, which spans from 420 to 540 nm with a maximum at ~460 nm, is related to transition from the $^6P_{3/2}$ state of the $4f^65d^1$ excited-configuration to the $^8S_{7/2}$ ground-state of Eu^{2+} ions. The characteristic blue afterglow is clearly seen for this sample. It results in the variation of the color properties, with CIE coordinates $x = 0.256$, $y = 0.165$ that fall into the purple region.

The decay of red (610 nm, the $^5D_0 \rightarrow ^7F_2$ transition) PL of Eu^{3+} ions under direct excitation at 532 nm to the 5D_1 state is analyzed in Fig. 10. The curves are plotted in a semi-log scale; so, for one type of sites for all Eu^{3+} ions the single-exponential decay is expected, which should be represented by a linear law. For the initial glass, the decay curve is near-linear; the lifetime of the 5D_0 state is 0.69 ms. After the heat-treatment of the glass at 720–740 °C for 6 h, decay curves clearly deviate from the single-exponential law, showing that Eu^{3+} ions partly enter the T-(Y,Yb,Eu)NbO₄ phase, partly remain in the residual glass. As a result, the decay contains a fast component with a characteristic time of

~140 μs , and a slow component with a decay time of ~0.7 ms corresponding to Eu^{3+} ions in the orthoniobate crystals and residual glassy phase, respectively. For the sample heat-treated at 800 $^{\circ}\text{C}$, the decay is again single-exponential, the lifetime of the $^5\text{D}_0$ state is 140 μs . It means that near all Eu^{3+} ions enter the T-phase crystals. For the heat-treatment at 900 $^{\circ}\text{C}$, the lifetime is slightly longer, 172 μs . This heat-treatment corresponds to the increase of mean diameter of the T-(Y,Yb,Eu) NbO_4 nanocrystals (so that the fraction of Eu^{3+} ions located in the nanocrystal “core” with the reduced non-radiative path is higher, as compared with the crystal-glass defect boundary). For the glass heat-treated at 1000 $^{\circ}\text{C}$, the decay time is 195 μs ; the change is attributed not only to the crystal growth but also to the beginning of crystallization of M-(Y,Yb,Eu) NbO_4 crystals. For M-YNbO₄:Eu nanocrystalline powder this value is 0.68 ms [58].

With 960 nm excitation, the PL spectra of Yb^{3+} ions ($^2\text{F}_{5/2} \rightarrow ^2\text{F}_{7/2}$ transition) are shown in Fig. 11. For the initial glass, an intense peak centered at 976 nm dominates over the plateau spanning across 990–1030 nm. Heat-treatments at 720–900 $^{\circ}\text{C}$ lead to a slight blue-shift of this peak to 974.5 nm, as well as to the reduction of its relative intensity. For the glass-ceramics heat-treated at 1000 $^{\circ}\text{C}$, the local peak at 1004 nm dominates the spectrum. The corresponding decay curves are shown in Fig. 12 (PL was excited at 975 nm and monitored at 1030 nm), for the initial glass and glass-ceramics. For the comparison, we present the positions of luminescence peaks of the already mentioned 5 at% Yb:YNbO₄ single crystal [60]. The peaks are at 955, 974, 1005, 1021 and 1030 nm, which is very similar to peaks Yb^{3+} in the luminescence spectrum of (Eu,Yb,Y) NbO_4 . The measured lifetime of the $^2\text{F}_{5/2}$ state for the initial glass is 0.68 ms; the heat-treatment of the glass at 720–740 $^{\circ}\text{C}$ results in the shortening of the overall “effective” decay time due to emerging the fast component with a decay time of ~100 μs . This is especially clear for the sample heat-treated at 740 $^{\circ}\text{C}$ for 24 h where the impact of both “fast” and “slow” components is compatible. For the sample heat-treated at 900 $^{\circ}\text{C}$, fast component is dominating in the decay curve; the $^2\text{F}_{5/2}$ lifetime is 95 μs . The heat-treatment at 1000 $^{\circ}\text{C}$ induces further lifetime shortening to 90 μs . Lifetime for 5 at% Yb:YNbO₄ single crystal is 0.9 ms [60]. The observed spectral and temporal behavior of PL of Yb^{3+} ions supports the conclusions about their entering into the RENbO₄ phase.

3.5 Up-conversion

The spectra of red up-conversion emission from the studied glass and glass-ceramics under near-IR (~960 nm) excitation are shown in Fig. 13a. They are related to $^5\text{D}_0 \rightarrow ^7\text{F}_J$ ($J = 0, 1, 2$ and 4)

transitions for Eu^{3+} ions; spectral positions, shapes and relative intensities of observed bands perfectly correspond to intrinsic emissions of Eu^{3+} under UV excitation, see Fig. 9a.

The scheme of this up-conversion process is shown in Fig. 14. The energy of the ${}^2\text{F}_{7/2}$ excited state of Yb^{3+} is near two times lower than that of the metastable ${}^5\text{D}_0$ state of Eu^{3+} , so the direct energy transfer (ET) cannot occur. However, in ytterbium-doped glass and glass-ceramics two close Yb^{3+} ions can form a pair with a "virtual" excited state. The energy of this state will be $2E({}^2\text{F}_{7/2})$ that is close to the energy of ${}^5\text{D}_1$ state of Eu^{3+} . Thus, a cooperative ET from an excited Yb^{3+} ion pair to a single Eu^{3+} ion is possible, followed by a fast non-radiative relaxation to the metastable ${}^5\text{D}_0$ state; and red Eu^{3+} emissions are observed. In Fig. 14, we depict also the possible ways of excitation of Eu^{3+} and Eu^{2+} ions in the studied materials, as well as their red and blue emission.

The efficiency of the cooperative ET $\text{Yb}^{3+} \rightarrow \text{Eu}^{3+}$ can be estimated by measuring the lifetime of luminescence of donor ions ($\text{D} = \text{Yb}^{3+}$ in our case) for the material singly doped with donor ions (i.e., singly Yb^{3+} -doped) and for the material codoped with donor and acceptor ($\text{A} = \text{Eu}^{3+}$ in our case) ions, i.e., ($\text{Yb}^{3+}, \text{Eu}^{3+}$)-codoped, in our case. Then, the ET efficiency, $\eta_{\text{ET}} = 1 - \tau_{\text{D}}/\tau_{\text{D-A}}$ where τ_{D} and $\tau_{\text{D-A}}$ are the corresponding lifetimes. In order to determine the τ_{D} lifetimes, we have prepared glasses and glass-ceramics singly doped with Yb^{3+} ions with the same heat-treatment regimes (the initial glass was doped with 1.5 mol% Yb_2O_3 , 1.7 mol% Y_2O_3 and 3.2 mol% Nb_2O_5). The efficiency of the ET, η_{ET} , slightly increases with the heat-treatment temperature in the range from $\sim 7 \pm 2\%$ for the initial glass to $\sim 15 \pm 3\%$ for the glass-ceramics heat-treated at 900 °C. This increase is attributed to a stronger interaction of active ions within the nanocrystals with an increased local concentration of RE ions.

To confirm the mechanism of up-conversion luminescence (UCL), we studied the dependency of the integrated UCL intensity, I_{UCL} , on the excitation power P . These plots for the initial glass and glass-ceramics heat-treated at 1000 °C are shown in Fig. 13 in a log-log scale to reveal the number of pump photons involved (n), as $I_{\text{UCL}} \sim P^n$ [76]. The points are the experimental data, lines are their approximation for the slope (that corresponds to n value) calculation. For both the initial glass and glass-ceramics, the values of n are 1.8–2.0, confirming a two-photon excitation mechanism.

In addition to Eu^{3+} UCL, we observed two types of "parasitic" emissions from the studied samples under near-IR excitation, Fig. 13b. The first one is UCL from Er^{3+} and Tm^{3+} ions presented as impurity in the Yb_2O_3 reagent. Blue emission at ~ 480 nm is related to the ${}^1\text{G}_4 \rightarrow {}^3\text{H}_6$ transition for the Tm^{3+} ions excited via the direct ET from Yb^{3+} ions. Similarly, ET $\text{Yb}^{3+} \rightarrow \text{Er}^{3+}$ and subsequent excited-state absorption are responsible for the excitation of Er^{3+} ions to the ${}^2\text{H}_{11/2} + {}^4\text{S}_{3/2}$ states (resulting in

green emission at ~520–540 nm), and to the $^4F_{9/2}$ state (resulting in red emission at ~650 nm). The second type of “parasitic” emission was detected only for the initial glass; this is the so-called cooperative luminescence from excited Yb^{3+} ion pairs. In Fig. 13b, the calculated emission spectrum of Yb^{3+} pairs is also shown, it is marked with an asterisk. The above mentioned factors change the color properties of UCL. For the initial glass, CIE coordinates are $x = 0.388$ and $y = 0.337$ (“warm” white light). For the sample heat-treated at 1000 °C, $x = 0.261$ and $y = 0.351$ (bluish light). Thus, elimination of the above mentioned effects is required for the obtaining of “pure” red UCL under near-IR excitation. On the other hand, proper Eu/Er/Tm codoping can be the route for warm/cold white light generation. This will be the topic of further research.

4. Discussion

Though there are two stable modifications of ReNbO_4 , low-temperature M- and high-temperature T-phases, in our previous study of glass-ceramics with $(\text{Er},\text{Yb})\text{NbO}_4$ nanosized crystals, we demonstrated for the first time crystallization of disordered fluorite-type T'-phase, that transforms to T- and then to M-phase upon heat-treatments [68]. The same character of phase transformations is found in the present study upon crystallization of $(\text{Y},\text{Yb},\text{Eu})\text{NbO}_4$ nanosized crystals.

The comparison of the DSC curve with the XRD patterns proves that the first exothermal peak is due to crystallization of $(\text{Y},\text{Yb},\text{Eu})\text{NbO}_4$. The second, intense exothermal peak reflects crystallization of the main crystalline phase, β -quartz ss. The third weak peak probably reflects the structural transformation of the $(\text{Y},\text{Yb},\text{Eu})\text{NbO}_4$ phase. Thus, $(\text{Y},\text{Yb},\text{Eu})\text{NbO}_4$ crystalline phase serves the nucleation centers for the volume crystallization of the lithium aluminosilicate crystalline phase of β -quartz ss.

The Raman spectroscopy findings prove these structural transformations. In the Raman spectrum of the initial glass (Figs 6 and 7) the broad bands about 490 and 870 (895 cm^{-1}) are due to vibrations of the aluminosilicate glass network with a large number of non-bridging oxygens [77] and of $[\text{NbO}_4]$ and $[\text{NbO}_6]$ polyhedrals [78], respectively. The band at $\sim 970\text{ cm}^{-1}$ (Fig. 7) corresponds to the vibrations of $[\text{SiO}_4]$ tetrahedra for which the scattering cross-section is substantially smaller than for the vibrations of the niobium-containing groups and therefore, its contribution to the band 870 cm^{-1} is small.

A number of spectral changes that occur at the early stages of heat-treatments at 720 and 740 °C for 6 hours, the emergence of a very weak broad band at about $250\text{-}350\text{ cm}^{-1}$, as well as appearance

and strengthening of the band at 805 cm^{-1} , reveal the formation of orthoniobate T' - RENbO_4 crystals with disordered fluorite-type structure [68, 80]. For interpretation of Raman spectra we used data on Raman spectra of crystalline yttrium, europium and ytterbium orthoniobates and of yttrium orthoniobate doped with europium and ytterbium. As should be noted, the samples exhibited very complex but similar spectra, as anticipated for identical crystal structures [72].

After raising the heat-treatment temperature to $800\text{ }^\circ\text{C}$, the glass matrix crystallizes in the form of β -quartz ss (the corresponding Raman bands appear at 110 cm^{-1} (not shown here) 480 and 1085 cm^{-1} [69,70]. The Raman spectrum gives the evidence of crystallization of tetragonal ReNbO_4 crystals (the bands at 340 , 658 cm^{-1} , 805 cm^{-1} and ~ 120 and $\sim 200\text{ cm}^{-1}$ (external modes) [81,82]) and of the absence of T' -phase (the disappearance of the broad band at about 300 cm^{-1}). These data are in accordance with the XRD findings.

Raman spectra of tetragonal and monoclinic rare-earth niobates are very similar and differ only in the three bands, which arise in the spectrum of the monoclinic phase due to lowering of the symmetry of the tetragonal crystal at the transition to the monoclinic one, i.e., intense band 238 cm^{-1} and two weak bands at about 420 cm^{-1} and about 695 cm^{-1} [72]. After the heat-treatment at $1000\text{ }^\circ\text{C}$ for 6 h, the crystallinity fraction of both orthoniobate and aluminosilicate crystalline phases increases as intensity of the characteristic bands raises. The bands of the β -quartz ss, the bands of the tetragonal YNbO_4 , and a number of bands specific for the monoclinic YNbO_4 : intense band 238 cm^{-1} , 695 cm^{-1} and two weak bands ~ 200 and $\sim 420\text{ cm}^{-1}$ (the shoulder of the intensive band at 480 cm^{-1}) appear in the Raman spectrum of the sample [72]. According to G. Blasse [82], Raman bands at 805 and 340 cm^{-1} are due to Nb-O symmetric modes of the NbO_4 tetrahedral structure, and Raman bands appearing at 658 and 420 cm^{-1} are due to Nb-O antisymmetric modes of the NbO_4 tetrahedral structure. The phonon energies below 300 cm^{-1} are assigned to external vibrations. Thus, according to Raman spectroscopy findings one may conclude that in the sample heat treated at $1000\text{ }^\circ\text{C}$ for 6 h the tetragonal and monoclinic crystals of RENbO_4 coexist.

In the lattice of Eu,Yb-doped yttrium niobate YNbO_4 , the doped luminescent center, Eu^{3+} and Yb^{3+} ions occupy the Y sites [60, 61], solid solutions are formed. The phase transformations are reflected in optical properties of glass-ceramics. All absorption and luminescence spectra can be divided into three groups. Spectra of initial glass and glass-ceramics with disordered fluorite-type structure demonstrate broad structureless bands characteristic for fluorite-type T' -orthoniobate crystals related to the local structural disorder and multiple Eu^{3+} and Yb^{3+} sites in the crystals with a defect fluorite-type

structure. According to the luminescence decay time measurements, the rare-earth ions are distributed between the crystalline and amorphous phases. Bands in spectra of glass-ceramics with tetragonal orthoniobate crystals appeared upon heat-treatments at 740 °C for 24 h, at 800 and 900 °C for 6 h are split and structured. According to the decay time measurements, all Eu^{3+} ions already enter the crystalline phase at 800 °C. In contrast, the heat-treatment at 1000 °C results in a sharp change of spectra. This clearly supports the beginning of transformation to the monoclinic (Y,Yb,Eu)NbO₄ phase. The single-exponent character of decay curves for glass-ceramics containing both T- and M-phases is probably connected with similar values of decay times for both crystal phases.

Electric-dipole (ED) hypersensitive transition 0→2 is the indicator of the symmetry of the local field for Eu^{3+} ions [5,83]. If the site for Eu^{3+} has no inversion center, this band dominates over the one related to the 0→1 magnetic-dipole (MD) transition. If the site has an inversion center, the 0→1 MD transition will be dominant. The relation $R = I_{(0\rightarrow2)\text{ED}}/I_{(0\rightarrow1)\text{MD}}$ is called the asymmetry parameter [5,6]. However, asymmetry parameter does not provide complete information about the symmetry of Eu^{3+} site which should be analyzed based on the structural studies; this work is in progress.

For the initial glass, the most intense PL band corresponds to the 0→2 ED transition, which is typical for glasses [6]. The corresponding R value is 6.5. The photoluminescence spectrum of the initial glass resembles that for the three-component lithium aluminosilicate glass containing 15 mol% Li₂O and 15 mol% Al₂O₃ and doped with 0.2 mol% Eu₂O₃ [26]. For that glass the estimated $R = 4.4$ [26]. The heat-treatment of the initial glass at 720–740 °C for 6 h leading to the precipitation of disordered fluorite-type T'- phase, does not change the symmetry of the local field around Eu^{3+} ions, which reflects the distortion of the surrounding of these ions in the T'- phase. It is interesting that in spite of the similarity of XRD patterns, the distortion of the local symmetry around Eu^{3+} ions in the T'-fluorite type phase is much higher than in nanoparticles based on ZrO₂ and Eu₃NbO₇ formed as a single phase of structure corresponding to cubic phase, for which R is near 1 [84].

The heat-treatment of the initial glass at 800–900 °C leading to the precipitation of T-orthoniobate phase, does not change the dominant role of the 0→2 emission channel, as there is no inversion center in the tetragonal RE niobate structure. The value of asymmetry parameter becomes even higher, $R = 8.0$. Finally, the beginning of precipitation of M-phase for the glass heat-treated at 1000 °C, again does not disturb the intensity distribution for ED and MD transitions (inversion center is not presented for Eu^{3+} ions in the monoclinic RENbO₄ structure); and $R = 7.6$. For the comparison, monoclinic nanocrystalline solid solutions in the YNbO₄–EuNbO₄ system demonstrate strong red lu-

minescence with main emission band at 610 nm and small orange luminescence with band at 590 nm, $R = 4 - 5.7$ depending on the preparation conditions [60]. It is worth noting that the authors did not notice any reduction of Eu^{3+} to Eu^{2+} in spite of the high heat-treatment temperature of 1300 °C [60].

5. Conclusions

Transparent glass-ceramics based on nanosized crystals of rare-earth orthoniobates, $(\text{Eu}^{3+}, \text{Yb}^{3+})$: YNbO_4 , and β -quartz ss were prepared and their spectral-luminescent properties were described for the first time. Upon heat-treatment at 720–740 °C, nanosized crystals of RENbO_4 with a defect fluorite structure (T'-phase) crystallize within the initial glass. Upon increase of temperature or time of the heat-treatments, size and volume fraction of these crystals increases; in the process, the crystal structure transforms to the tetragonal one, T-phase. Then, at 1000 °C the transformation to the monoclinic form (M-phase) begins. Rare-earth niobates act as nucleating agents for bulk crystallization of β -quartz solid solutions, the main crystalline phase of glass-ceramics, which starts to crystallize at 740°C.

Optical properties of glass-ceramics are directly linked to crystallization and the structure of rare-earth niobates. Analysis of luminescence parameters of glass-ceramics led to conclusion that under heat-treatment at 800 °C almost all Eu^{3+} and Yb^{3+} ions enter the niobate crystals and a partial reduction of Eu^{3+} to Eu^{2+} ions is observed at 1000 °C. Rare-earth orthoniobates provide promising spectral-luminescent properties while the large amount of the main crystalline phase of β -quartz ss ensures high thermal shock resistance of the glass-ceramics. Based on the results obtained in the present work for Eu^{3+} ions and $(\text{Eu}^{3+}, \text{Yb}^{3+})$ couple and our previous results for Yb^{3+} and $(\text{Er}^{3+}, \text{Yb}^{3+})$ ions [69] in RENbO_4 nanocrystals, we conclude that RENbO_4 -based transparent glass-ceramics are very interesting as a matrix for further double $(\text{RE}^{3+}, \text{Yb}^{3+})$ or triple $(\text{RE}_1^{3+}, \text{RE}_2^{3+}, \text{Yb}^{3+})$ codoping for color-tunable phosphors in the visible and for generation of warm/cold white light. Further work to determine the radiation quantum efficiency and non-radiative relaxation rates for RE^{3+} ions is required to quantify the performance of RENbO_4 -based glass-ceramics.

Acknowledgements

This work was partially supported by the RFBR (Grant 16-03-01130) and performed under the task of Ministry of Education and Science of Russian Federation (task No. 3.109.2014/K). The au-

thors wish to express their deep gratitude to Mr. Sobolev for his help in the glass synthesis, and to Ms Vasilevskaya for recording the DSC curve.

References

1. G. Wakefield, E. Holland, P.J. Dobson, J.L. Hutchison, *Adv. Mater.* 13 (2001) 1557–1560.
2. T. Igarashi, M. Ihara, T. Kusunoki, K. Ohno, T. Isobe, M. Senna, *Appl. Phys. Lett.* 76 (2000) 1549–1551.
3. P.A. Loiko, V.I. Dashkevich, S.N. Bagaev, V.A. Orlovich, A.S. Yasukevich, K.V. Yumashev, N.V. Kuleshov, E.B. Dunina, A.A. Kornienko, S.M. Vatik, A.A. Pavlyuk, *Laser Phys.* 23 (2013) 105811-1–7.
4. A.F. Kirby, F.S. Richardson, *J. Phys. Chem.* 87 (1983) 2544–2556.
5. K. Binnemans, C. Görller-Walrand, 14 (1996) 173–180.
6. R. Reisfeld, E. Zigansky, M. Gaft, 102 (2004) 1319–1330.
7. M. Peng, Z. Pei, G. Hong, Q. Su, *Chem. Phys. Lett.* 371 (2003) 1–6.
8. Z. Pei, Q. Su, J. Zhang, *J. Alloys Compd.* 198 (1993) 51–53.
9. K. Machida, D. Ueda, S. Inoue, G. Adachi, *Chem. Lett.* 28 (1999) 785 – 786.
10. S. Liu, G. Zhao, W. Ruan, Z. Yao, T. Xie, J. Jin, H. Ying, J. Wang, G. Han, *J. Am. Ceram. Soc.* 91 (2008) 2740–2742.
- 11 6. K.B. Kim, Y.I. Kim, H.G. Chun, T.Y. Cho, J.S. Jung, J.G. Kang, *Chem. Mater.* 14 (2002) 5045–5052.
12. L.R. Dačanin, M.D. Dramičanin, S.R. Lukič-Petrovič, D.M. Petrovič, M.G. Nikolič, *Radiat Meas* 56 (2013) 143–146.
13. E. Pavitra, G. Seeta Rama Raju, J.S. Yu, *Phys. Status Solidi RRL* 7 (2013) 224–227.
14. J. Zhao, H. Duan, Z. Ma, T. Wang, C. Chen, E. Xie, *J. Appl. Phys.* 104 (2008), 053515.
15. N. Rakov, G.S. Maciel, W. Lozano B., C.B. de Araújo, *J. Appl. Phys.* 101 (2007) 036102.
16. R. Hao, Q. Meng, W. Liu, H. Liu, *J. Rare Earth* 31 (2013) 864–870.
17. G.E. Malashkevich, G.P. Shevchenko, Yu.V. Bokshits, A.A. Kornienko, P.P. Pershukevich, *Opt. Spectrosc.* 98 (2005) 190–194.
18. A. Lukowiak, R.J. Wiglusz, A. Chiappini, C. Armellini, I.K. Battisha, G.C. Righini, M. Ferrari, *J. Non-Cryst. Solids* 401 (2014) 32–35.
19. A. Nishikawa, T. Kawasaki, N. Furukawa, Y. Terai, Y. Fujiwara, *APEX*, 2 (2009) 071004-1–3.
20. M. Gaft, R. Reisfeld, G. Panczer, S. Shoval, B. Champagnon, G. Boulon, *J. Lumin.* 72-74 (1997) 572–574.

21. K.H. Jang, E.S. Kim, L. Shi, N.M. Khaidukov, H.J. Seo, *Opt. Mater.* 31 (2009) 1819–1821.
22. R. Yavetskiy, A. Tolmachev, M. Dubovik, T. Korshikova, S. Parkhomenko, *Opt. Mater.* 30 (2007) 119–121.
23. V. Venkatramu, P. Babu, C.K. Jayasankar, *Spectrochim. Acta, Part A*, 63 (2006) 276–281.
24. W.A. Pisarski, J. Pisarska, G. Dominiak-Dzik, M. Maćzka, W. Ryba-Romanowski, *J. Phys. Chem. Solids* 67 (2006) 2452–2457.
25. A. Ruivo, V.S.F. Muralha, H. Águas, A. Pires de Matos, C.A.T. Laia, *J. Quant. Spectrosc. Radiat. Transfer* 134 (2014) 29–38.
26. A. Herrmann, S. Kuhn, M. Tiegel, C. Rüssel, *Opt. Mater.* 37 (2014) 293–297.
27. T. Qin, G. Mountjoy, N.D. Afify, M.F. Reid, Y.Y. Yeung, A. Speghini, M. Bettinelli, *Phys. Rev. B* 84 (2011) 104206.
28. D. Chen, Y. Wang, N. Yu, P. Huang, *J. Phys. Chem. C* 112 (2008) 18943–18947.
29. S. Taruta, M. Matsuki, H. Nishikiori, T. Yamakami, T. Yamaguchi, K. Kitajima, *Ceram. Int.* 36 (2010) 1303–1309.
30. G. Gao, N. Da, S. Reibstein, L. Wondraczek, *Opt. Express*, 18 (2010) A575–583.
31. Y. Yu, F. Weng, D. Chen, P. Huang, Y. Wang, *J. Appl. Phys.* 107 (2010) 093504.
32. Y. Hatefi, N. Shahtahmasebi, A. Moghimi, E. Attaran, *J. Lumin.* 131 (2011) 114–118.
33. G. Gao, S. Reibstein, M. Peng, L. Wondraczek, *J. Mater. Chem.* 21 (2011) 3156–3161.
34. R. Bagga, V.G. Achanta, A. Goel, J.M.F. Ferreira, N.P. Singh, D.P. Singh, V. Contini, M. Falconieri, G. Sharma, *Opt. Mater.* 36 (2013) 198–206.
35. F. Hu, X. Wei, S. Jiang, S. Huang, Y. Qin, Y. Chen, C.-K. Duan, M. Yin, *J. Amer. Ceram. Soc.* 98 (2015) 464–468.
36. H. Guo, F. Li, J. Li, H. Zhang, *J. Am. Ceram. Soc.*, 94 (2011) 1651–1653.
37. H. Guo, X. Liu, F. Li, R. Wei, Y. Wei, C. Ma, *J. Electrochem. Soc.* 159 (2012) J223–J226.
38. H. Wang, C. Duan, P.A. Tanner, *J. Phys. Chem. C* 112 (2008) 16651–16654.
39. X. Wei, J. Zhao, W. Zhang, Y. Li, M. Yin, *J. Rare Earth* 28 (2010) 166–170.
40. R. Martin-Rodriguez, R. Valiente, S. Polizzi, M. Bettinelli, A. Speghini, F. Piccinelli, *J. Phys. Chem. C* 113 (2009) 12195–12200.
41. V. Jubera, A. Garcia, J.P. Chaminade, F. Guillen, J. Sablayrolles, C. Fouassier, *J. Lumin.* 124 (2007) 10–14.
42. Y. Dwivedi, D.K. Rai, S.B. Rai, *Opt. Mater.* 32 (2010) 913–919.
43. W. Streck, P.J. Deren, A. Bednarkiewicz, Y. Kalisky, P. Boulanger, *J. Alloys Comp.* 300–301 (2000) 180–183.

44. Y. Dwivedi, S.N. Thakur, S.B. Rai, *Appl. Phys. B* 89 (2007) 45–51.
45. P.A. Loiko, G.E. Rachkovskaya, G.B. Zakharevich, K.V. Yumashev, *Glass Ceram.* 71 (2014) 41–44.
46. P.A. Loiko, G.E. Rachkovskaya, G.B. Zakharevich, A.A. Kornienko, E.B. Dunina, A.S. Yasukevich, K.V. Yumashev, *J. Non-Cryst. Solids* 392-393 (2014) 39–44.
47. G.S. Maciel, A. Biswas, P.N. Prasad, *Opt. Commun.* 178 (2000) 65–69.
48. Y. Dwivedi, A. Rai, S.B. Rai, *J. Lumin.* 129 (2009) 629–633.
49. P.A. Loiko, G.E. Rachkovskaya, G.B. Zakharevich, K.V. Yumashev, *Opt. Spectrosc.* 118 (2015) 235–239.
50. A. Bahadur, Y. Dwivedi, S.B. Rai, *Spectrochim. Acta, Part A* 91 (2012) 217–221.
51. Q. Luo, X. Qiao, X. Fan, H. Fu, J. Huang, Y. Zhang, B. Fan, X. Zhang, *J. Am. Ceram. Soc.* 95 (2012) 1041–1047.
52. K Biswas, S Balaji, D Ghosh, AD Sontakke, K Annapurna, *J. Alloys Compd.* 608 (2014) 266-271.
53. Y. Zhou, Q. Ma, M.Lü, Z.Qiu, A. Zhang, *J. Phys. Chem. C* 112 (2008) 19901–19907.
54. G. Blasse, *J. Lumin.* 14 (1976) 231–233.
55. O.A. Serra, S.A. Cicillini, R.R. Ishiki, *J. Alloy Compd.* 303-304 (2000) 316–319.
56. A.M.G. Massabni, G.J.M. Montandon, M.A. Couto dos Santos, *Materials Research*, 1 (1998) 1-4.
57. E.Y. Lee, Y.J. Kim, *J. Korean Electrochem. Soc.* 12 (2009) 234–238.
58. Lj.R. Đačanin, M.D. Dramićanin, S.R. Lukić-Petrović, D.M. Petrović, M.G. Nikolić, T.B. Ivetić, I.O. Gúth, *Ceram. Int.* 40 (2014) 8281-8286.
59. Lj.R. Đačanin, S.R. Lukić-Petrović, D.M. Petrović, M.G. Nikolić, M. D. Dramićanin, *J. Lumin.* 151 (2014) 82–87.
60. M. Hirano, H. Dozono, *Mater. Res. Bull.* 50 (2014) 213–220.
61. P.Y. Zhou, Q.L. Zhang, H.J. Yang, K.J. Ning, D.L. Sun, J.Q. Luo, S.T. Yin, *Acta Phys. Sin.* 61 (2012) 228103.
62. M.P.F. Graça, M.V. Peixoto, N. Ferreira, J. Rodrigues, C. Nico, F. M. Costa, T. Monteiro, *J. Mater. Chem. C1* (2013) 2913–2919.
63. J. Hou, Q. Chen, C. Gao, R. Dai, J. Zhang, Z. Wang, Z. Zhang, Z. Ding, *J. Rare Earth* 32 (2014) 787–791.
64. K.U. Kumar, N. Vijaya, J. Oliva, C. Jacinto, E. de La Rosa, C.K. Jayasankar, *Mater. Express* 2 (2012) 294-302.
65. A.I. Komkov, *Doklady Akad. Nauk SSSR* 126 (1959) 853-854.
66. K. Jurkschat, P. Sarin, L. F. Siah, W.M. Kriven, *Advances in X-ray Analysis* 47 (2004) 357.

67. V. Stubican, *J. Am. Ceram. Soc.* 47 (1964) 55-58.
68. S.A. Mather, P.K. Davies, *J. Am. Ceram. Soc.* 78 (1995) 2737-2745.
69. O.S. Dymshits, I.P. Alekseeva, A.A. Zhilin, M.Ya. Tsenter, P.A. Loiko, N.A. Skoptsov, A.M. Malyarevich, K.V. Yumashev, X. Mateos, A.V. Baranov, *J. Lumin.* 160 (2015) 337–345.
70. I. Alekseeva, O. Dymshits, V. Ermakov, A. Zhilin, V. Petrov, M. Tsenter, *J. Non-Cryst. Solids* 354 (2008) 4932-4939.
71. H. Lipson, H. Steeple. *Interpretation of X-ray powder patterns*, ed. McMillan. London, N.Y., Martins Press, 1970.
72. K.P.F. Siqueira, R.L. Moreira, A. Dias, *Chem. Mater.* 22 (2010) 2668–2674.
73. P.A. Loiko, V.I. Dashkevich, S.N. Bagaev, V.A. Orlovich, A.S. Yasukevich, K.V. Yumashev, N.V. Kuleshov, E.B. Dunina, A.A. Kornienko, S.M. Vatnik, A.A. Pavlyuk, *J. Lumin.* 153 (2014) 221–226.
74. P. Naresh, G.N. Raju, Y. Gandhi, M. Piasecki, N. Veeraiah, *J. Am. Ceram. Soc.* 98 (2015) 413–422.
75. J. Tauc, *Amorphous and Liquid Semiconductors*, Plenum Press, London and New York, 1974.
76. M. Pollnau, D.R. Gamelin, S.R. Lüthi, H.U. Güdel, M.P. Hehlen, *Phys. Rev. B* 61 (2000) 3337-3346.
77. P. McMillan, *American Mineralogist* 69 (1984) 622-644.
78. G. Huanxin, W. Zhongcai, W. Shizhuo, *J. Non-Cryst. Solids* 112 (1989) 332-335.
80. M. Yashima, Jin-Ho Lee, M. Kakihana, M. Yoshimura, *J. Phys. Chem. Solids* 58 (1997) 1593-1597.
81. J-M. Jeng, I. E. Wachs, *Chem. Mater.* 3 (1991) 100-107.
82. G. Blasse, *J. Solid State Chem.* 7 (1972) 169-171.
83. P.A. Loiko, V.I. Dashkevich, S.N. Bagaev, V.A. Orlovich, X. Mateos, J.M. Serres, E.V. Vilejshikova, A.S. Yasukevich, K.V. Yumashev, N.V. Kuleshov, E.B. Dunina, A.A. Kornienko, S.M. Vatnik, A.A. Pavlyuk, *J. Lumin.* 168 (2015) 102–108.
84. M. Hirano, H. Dozono, *J. Ceram. Soc. Jpn.* 121 (2013) 113-115.

Figure captions

Fig. 1. Images of polished samples of initial glass and corresponding glass-ceramics. The values indicated in the figure denote heat-treatment schedule.

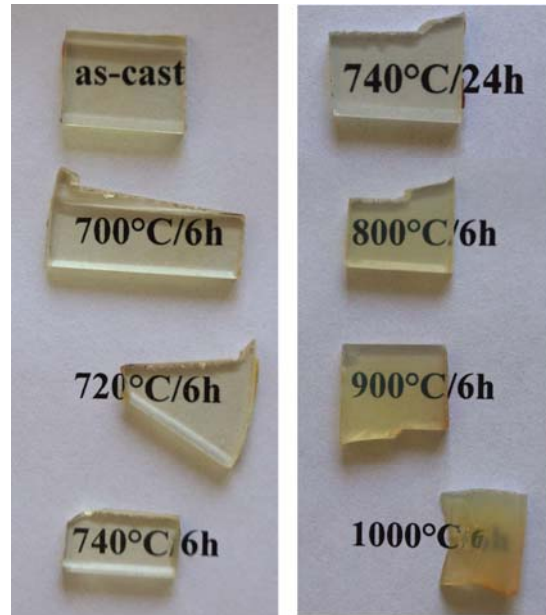


Fig. 2. DSC curve of the initial glass.

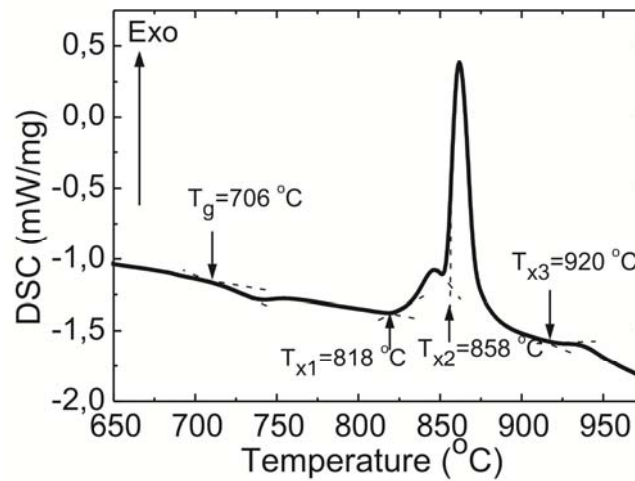


Fig. 3. XRD patterns of heat-treated glasses: (a) heat-treatment temperatures are 1 – 700 °C, 2 - 720 °C, 3 - 740 °C, 4 - 800 °C, 5 - 900 °C, 6 - 1000 °C and the duration is 6 h; (b) heat-treatment temperature is 740 °C and the duration is 6 and 24 h. The patterns are shifted for the convenience of observation.

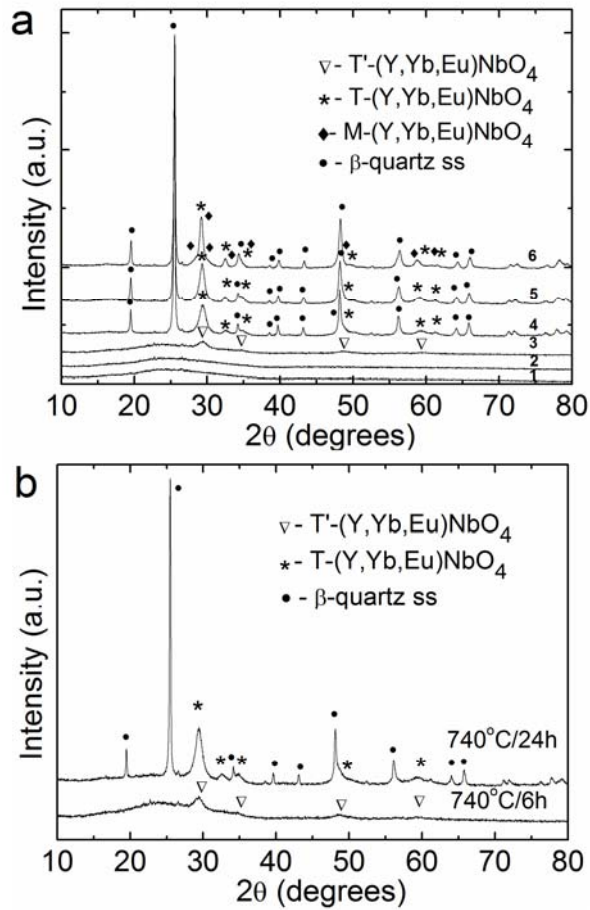


Fig. 4. TEM images of glass-ceramic samples heat-treated at 800 °C for 6 h (a) and at 900 °C for 6 h (b).

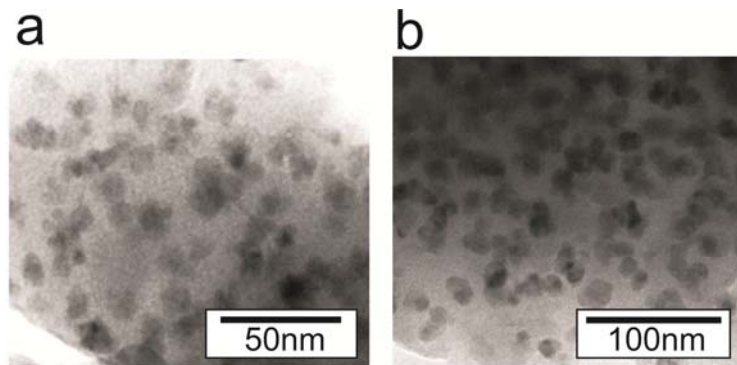


Fig. 5. Raman spectra of initial and heat-treated glasses: excitation wavelength $\lambda_{ex} = 488$ nm (a) and 514 nm (b). The values indicated in the figure denote heat-treatment temperatures, heat-treatment duration is 6 h. The spectra are shifted for the convenience of observation.

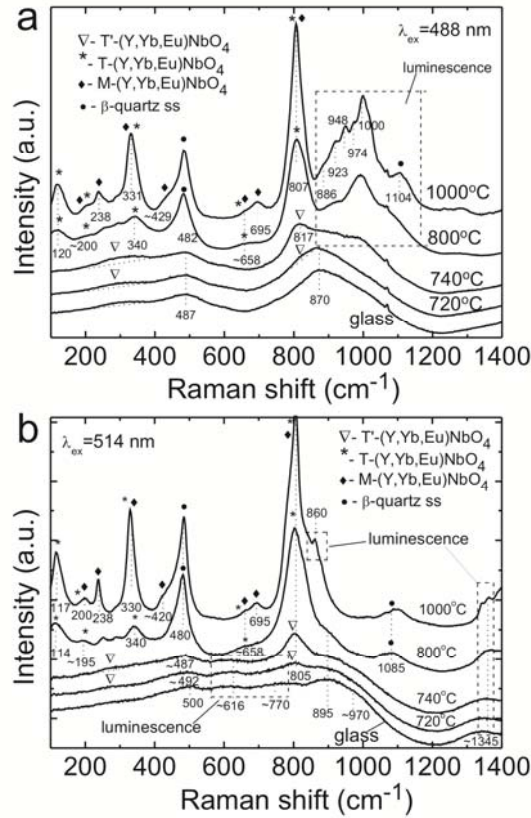


Fig. 6. Optical absorption spectra of Eu³⁺ and Yb³⁺ codoped glass and glass-ceramics (*inset* represents Tauc's plot for the initial glass and glass-ceramics). The values indicated in the figure denote heat-treatment schedules.

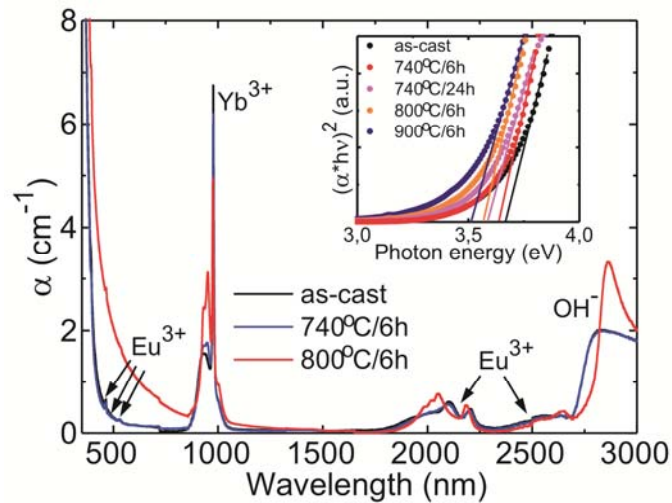


Fig. 7. The most intense absorption bands of Eu^{3+} ions in the visible related to transitions to the $^5\text{L}_6$, the $^5\text{D}_2$ and the $^5\text{D}_1$ excited-states for the initial glass and glass-ceramics; the spectra are shifted for the convenience of their comparison; the numbers denote heat-treatment schedules.

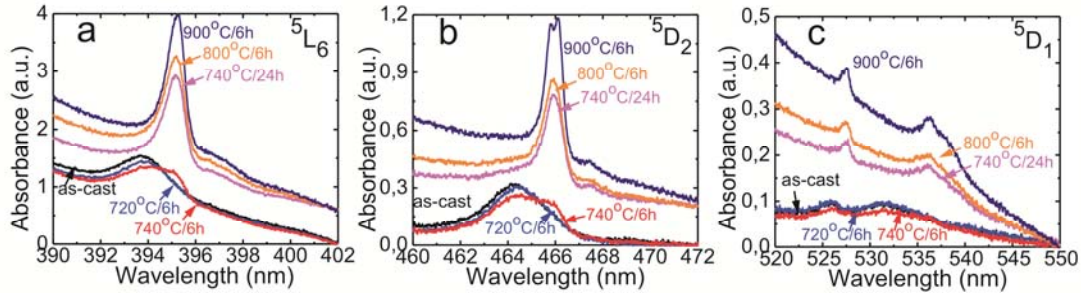


Fig. 8. Absorption band of Yb^{3+} ions (the $^2\text{F}_{7/2} \rightarrow ^2\text{F}_{5/2}$ transition) for the initial glass and glass-ceramics; the spectra are shifted for the convenience of their comparison; the numbers denote heat-treatment schedules.

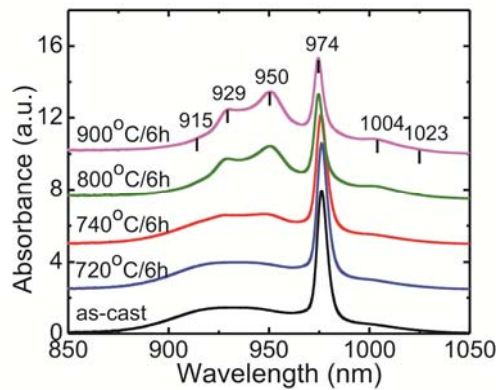


Fig. 9. (a) Photoluminescence (PL) related to Eu^{3+} ions under UV excitation to the $^5\text{L}_6$ state (~ 400 nm) for the initial glass and glass-ceramics. All spectra are normalized to unity to compare their shape and shifted for convenience of observation. The bands related to the $^5\text{D}_0 \rightarrow ^7\text{F}_j$ transitions are assigned; (b) structure of PL spectrum for the sample heat-treated at 1000°C for 6 h; *inset* represents emission band of Eu^{2+} ions, *asterisk* denotes emission from the $^5\text{D}_1$ state.

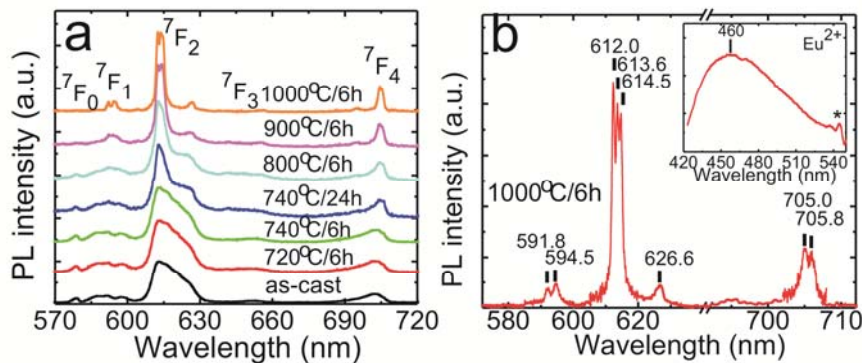


Fig. 10. The decay of red Eu^{3+} emission for the initial glass and glass- ceramics (excitation at 532 nm to the $^5\text{D}_1$ state).

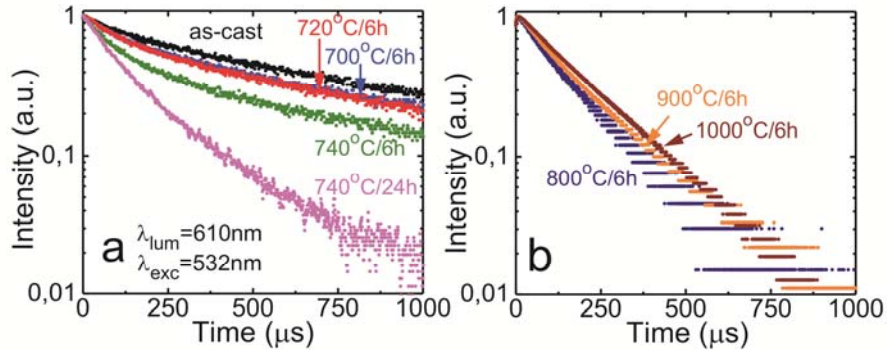


Fig. 11. PL spectra of Yb^{3+} ions (the $^2\text{F}_{5/2} \rightarrow ^2\text{F}_{7/2}$ transition) under excitation at 960 nm for the initial glass and glass-ceramics [not in scale].

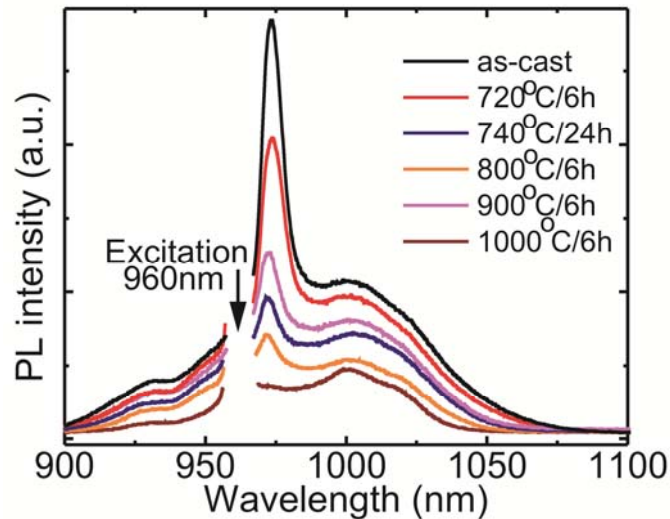


Fig. 12. The decay of near-IR Yb^{3+} emission for the initial glass and glass- ceramics (excitation at 960 nm).

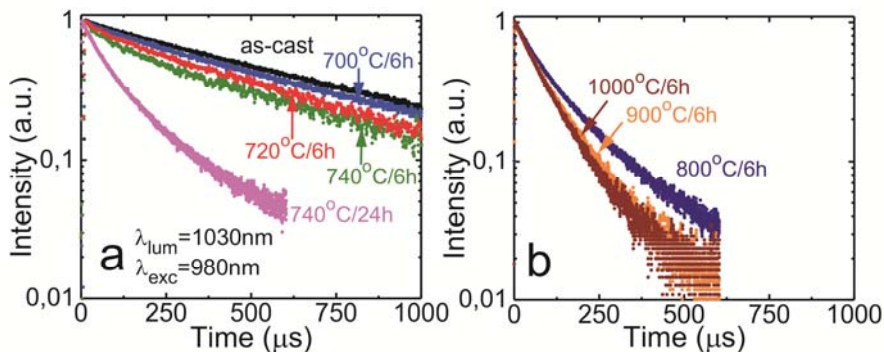


Fig. 13. (a) Up-conversion luminescence (UCL) spectra of the initial glass and glass-ceramics under 960 nm excitation; (b) UCL from impurity ions for the initial glass and glass-ceramics heat-treated at 1000 °C/6h; *asterisk* denotes the calculated emission spectrum for the Yb³⁺ pairs; (c,d) the log-log plots for UCL from the initial glass (c) and glass-ceramics (d) heat-treated at 1000 °C for 6 h.

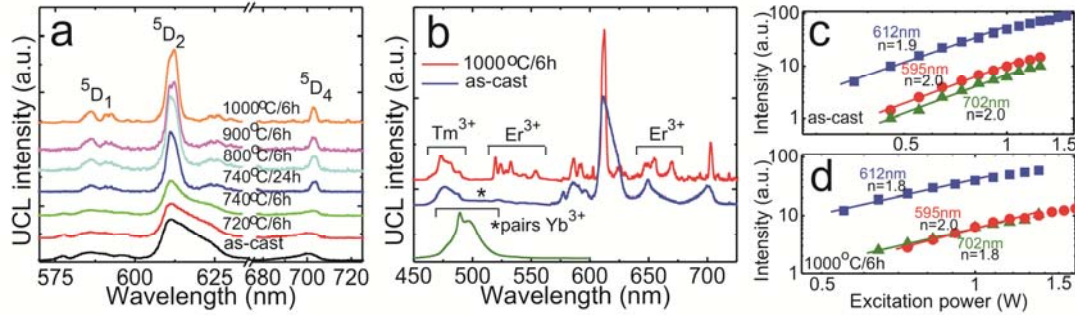


Fig. 14. Scheme representing excitation and emission channels of Eu³⁺ and Eu²⁺ ions in the studied glass-ceramics.

